Available online at www.sciencedirect.com
SCIENCE DIRECT
Journal of Catalysis 228 (2004) 66–74
JOURNAL OF CATALYSIS
www.elsevier.com/locate/jcat

Storage and supply of hydrogen by means of the redox of the iron oxides modified with Mo and Rh species

Sakae Takenaka *, Tomohiro Kaburagi, Chisa Yamada, Kiyoshi Nomura, Kiyoshi Otsuka *

Department of Applied Chemistry, Graduate School of Science and Engineering, Tokyo Institute of Technology, O-okayama 2-12-1, Meguro-ku, Tokyo 152-8552, Japan

Received 20 March 2004; revised 13 August 2004; accepted 17 August 2004

Available online 25 September 2004

Abstract

The redox performance of iron oxides containing Mo and/or Rh species ($Fe_3O_4 + 4H_2 \leftrightarrows 3Fe + 4H_2O$) was investigated. The redox cycle of the reduction of Fe_3O_4 with hydrogen and the subsequent oxidation of iron metal with water vapor can be applied for the storage and supply of pure hydrogen. Addition of Rh to the iron oxide samples improved the reactivity for the redox at a low temperature. The addition of Rh to iron oxide samples decreased apparent activation energy for the oxidation of iron metal with water vapor. However, Rh species added to iron oxides promoted sintering of iron species during the redox. The addition of Mo cations to iron oxides containing Rh prevented the sintering of iron species during the redox. Therefore, iron oxides containing both Rh and Mo species could form hydrogen repeatedly through the redox. The local structures of Mo and Rh species added to the iron oxide samples were investigated by Mo and Rh *K*-edge XANES and EXAFS. Mo cations added to the iron oxide samples were always stabilized in the ferrites $Mo_xFe_{3-x}O_4$ during the repeated redox reactions. Rh species added to the iron oxide samples were present as Rh–Fe alloys after the reduction with hydrogen, while they were present as Rh metal after the oxidation with H_2O.

Keywords: Iron oxides added with Mo and Rh; Redox of iron oxides; Hydrogen

1. Introduction

The redox property of a metal oxide is one of the factors which determine its catalytic activity and selectivity for a catalytic reaction. Frequently, various foreign metals or metal oxides, which are often termed as promoters, are added into the metal oxide catalysts in order to improve their redox performances [1–3]. In general, the surface areas of metal oxides decrease due to the sintering when they are used continuously in the catalytic reactions. The promoters sometimes prevent the sintering of the host metal oxide catalysts [4–6]. Therefore, the promoters are indispensable for the design of the catalysts for many catalytic reactions.

Previously, we have proposed a new method for the storage and supply of pure hydrogen by applying the redox between Fe_3O_4 and iron metal [7]:

$$Fe_3O_4 + 4H_2 \leftrightarrows 3Fe + 4H_2O. \quad (1)$$

Fe_3O_4 is reduced with hydrogen into iron metal by eliminating water from the system and subsequently the metal is oxidized with water vapor into Fe_3O_4 to form hydrogen. Hydrogen is stored chemically as Fe metal in this method. By means of this method, 1 mol of Fe can store and regenerate 1.33 mol of H_2, which corresponds to 4.8 wt% of Fe metal. However, iron oxide sample without any promoters was deactivated quickly for the hydrogen formation through the oxidation of iron metal with water vapor due to the sintering of Fe_3O_4 and/or iron metal [8]. In addition, the redox reaction of iron oxide sample without any promoters required relatively high temperatures (> 673 K). It is desirable to perform the redox reactions of iron oxide

* Corresponding authors. Fax: +81-3-5734-2879.
E-mail address: stakenak@o.cc.titech.ac.jp (S. Takenaka).

0021-9517/$ – see front matter
doi:10.1016/j.jcat.2004.08.027

samples at temperatures as low as possible from an economical viewpoint. Thus, the redox performances of the iron oxide samples added with various metal species were investigated [8,9]. Iron oxides added with Mo cations could form hydrogen repeatedly through the redox, while iron oxide without any promoters was deactivated quickly for the redox. The addition of Rh into iron oxides enhanced hydrogen formation through the oxidation of iron metal with water vapor at low temperatures. However, the role of these promoters on the redox of iron oxides has been unclear. The role of these promoters on the redox should be investigated on the bases of the local structures and the electronic states of metal species added into the iron oxides.

In the present study, the local structures and the electronic states of Rh and Mo species added into the iron oxide samples were investigated by Rh and Mo K-edge XANES and EXAFS. On the bases of these results, the roles of Rh and Mo species added into the iron oxide samples on the redox reactions between Fe_3O_4 and Fe metal will be discussed.

2. Experimental

Iron oxide without any promoters (denoted as FeO_x hereafter) was prepared by precipitation of $Fe(OH)_3$ from an aqueous solution of $Fe(NO_3)_3$ by using hydrolysis of urea at 363 K. The iron oxides added with Rh and/or Mo species (denoted as Rh–FeO_x, Mo–FeO_x and Rh–Mo–FeO_x hereafter) were prepared by coprecipitation of the corresponding metal hydroxides from mixed aqueous solutions containing these metal cations by using hydrolysis of urea at 363 K. $RhCl_3$ and $(NH_4)_6Mo_7O_{24}$ were used as metal sources. The precipitates were dried at 373 K for 12 h and calcined at 773 K for 10 h in air. The amount of Rh or Mo species added into iron oxides (Rh–FeO_x or Mo–FeO_x) was adjusted to be 5 mol% ($Rh/(Rh + Fe) = Mo/(Mo + Fe) = 0.05$ as mole ratio). When both Mo and Rh species were added into iron oxides, the content of Rh and Mo added was adjusted to be 5 mol% each in total metal atoms ($Rh/(Rh + Mo + Fe) = Mo/(Rh + Mo + Fe) = 0.05$ as mole ratio).

The reduction of iron oxides with hydrogen and the subsequent oxidation of iron metal with water vapor were carried out with a conventional gas-flow system with a fixed-bed reactor. Iron oxide sample was packed in a tubular reactor made from quartz (an inner diameter and lengths = 1.8 and 60 cm, respectively). The amount of the iron oxide samples packed in the reactor was 0.20 g as Fe. For the reduction, hydrogen diluted with Ar ($P(H_2) = P(Ar) = 50.7$ kPa, total flow rate = 100 ml min^{-1}) was contacted with the iron oxide sample at 573 K. The temperature at the reactor was increased linearly with time to 823 K at a rate of 7.5 K min^{-1} and the temperature was kept at 823 K until the consumption of hydrogen due to the reduction of iron oxides could not be observed. After the hydrogen remaining in the reactor was purged out with Ar, water vapor balanced with Ar ($P(H_2O) = 5.0$ kPa, total pressure = 101.3 kPa, total flow rate = 100 ml min^{-1}) was contacted with the reduced iron oxide samples at 373 K. The temperature at the reactor was increased linearly with time to 873 K at a rate of 4 K min^{-1}. The oxidation of the iron oxide samples with water vapor was continued at 873 K until the formation of hydrogen was not observed. During the oxidation with water vapor, a part of effluent gases from the catalyst bed was sampled out and analyzed by GC. The reduction with hydrogen and the subsequent oxidation with water vapor for the iron oxide samples were carried out repeatedly under the same conditions. XRD studies showed that iron species in all the fresh iron oxide samples used in the present study were Fe_2O_3 mainly, irrespective of the kind of promoters added into the iron oxide samples. The Fe_2O_3 in the fresh samples was reduced with hydrogen into iron metal at the first reduction. Subsequently the metal was oxidized into Fe_3O_4 at the first oxidation with water vapor. The oxidation of iron metal with water vapor to Fe_2O_3 was thermodynamically impossible. After the first cycles, the redox was performed between Fe_3O_4 and Fe metal.

X-ray absorption spectra (XANES, X-ray absorption near-edge structure; and EXAFS, extended X-ray absorption fine structure) were measured on the beam line BL-10B at the Photon Factory in the Institute of Materials Structure Science for High Energy Accelerator Research Organization at Tsukuba in Japan (Proposal Number 2002G108). Mo and Rh K-edge XANES and EXAFS of iron oxides added with Rh and Mo were measured with a transmission mode with a Si(311) channel-cut monochromator at room temperature. Mo–FeO_x and Rh–Mo–FeO_x were reduced with hydrogen at 823 K and they were subsequently oxidized with water vapor at 873 K prior to the measurement of XANES and EXAFS. After the redox reactions, the sample was packed in a bag made from polyethylene under Ar. The analysis of EXAFS data was performed by using an EXAFS analysis program, REX (Rigaku Co.). For EXAFS analysis, the oscillation was extracted from the EXAFS data by a spline-smoothing method. The oscillation was normalized by the edge height around 70–100 eV above the threshold. The Fourier transformation of k^3-weighted EXAFS oscillation was performed over a k-range of 3.5 to 14.5 $Å^{-1}$. Inversely Fourier-transformed data for each Fourier peak were analyzed by a curve-fitting method, using theoretically phase-shift and amplitude functions derived by FEFF8 program [10].

X-ray diffraction (XRD) patterns of iron oxide samples were recorded with a Rigaku RINT 2500V diffractometer using Cu-K_α radiation at room temperature under air.

SEM images of the iron oxide samples were measured with a Hitachi FE-SEM S-800 (field emission gun scanning electron microscope).

3. Results and discussion

3.1. Redox of iron oxides

The redox performances of FeO_x, Rh–FeO_x, Mo–FeO_x, and Rh–Mo–FeO_x were examined. For the reduction of these samples, hydrogen was contacted with these samples at 573 K and the temperatures at the reactor were increased to 823 K. After the reduction, the reduced samples were contacted with water vapor at 373 K and the temperature increased to 873 K. Five redox cycles were repeated for all the samples except for Rh–FeO_x. Fig. 1 shows change of the formation rate of hydrogen as a function of temperature at the reactor during the first oxidation, the third oxidation, and the fifth oxidation with water vapor of each sample. Iron oxide sample without promoters (FeO_x) produced hydrogen in the first oxidation with water vapor when temperatures became higher than 550 K. The formation rate of hydrogen for FeO_x increased with a rise of temperatures and it attained the maximum at around 780 K. However, the formation rates of hydrogen for FeO_x in the temperature range from 550 to 800 K became slower gradually with the repeated cycles. The deactivation of FeO_x for the oxidation with water vapor resulted from the sintering of iron species, as will be described below in detail. The deactivation of FeO_x for the hydrogen formation through the oxidation with water vapor was mitigated by the addition of Mo cations. The oxidation of Mo–FeO_x with water vapor produced hydrogen at temperatures higher than 550 K and the formation rate of hydrogen attained a maximum at around 650 K at the first oxidation with water vapor. The formation rate of hydrogen in the temperature range of 600 to 700 K for Mo–FeO_x was significantly higher than that for FeO_x. It should be noted that the kinetic curves of hydrogen formation for Mo–FeO_x did not change appreciably from the first oxidation to the fifth oxidation; i.e., the formation rates of hydrogen attained a maximum at around 650 K for every cycle of Mo–FeO_x, while the oxidation of FeO_x with water vapor required higher temperatures with the repeated cycles. On the other hand, the addition of Rh species into FeO_x enhanced the formation rate of hydrogen at low temperatures. The first oxidation of the Rh–FeO_x with water vapor formed hydrogen at temperatures higher than 500 K and the formation rate of hydrogen attained a maximum at ca. 600 K. The formation rates of hydrogen in the temperature range of 500 to 600 K at the first oxidation of Rh–FeO_x with water vapor were considerably higher than those at the first oxidation of FeO_x and Mo–FeO_x. However, the Rh–FeO_x was deactivated quickly for the hydrogen formation with the repeated cycles. The formation rate of hydrogen at the third oxidation of Rh–FeO_x with water vapor was very slow over the whole temperature range. As will be described below, the addition of Rh only into the iron oxides promoted the sintering of Fe_3O_4 and/or iron metal during the redox. Thus, the reactivity of Rh–FeO_x for the hydrogen formation in the third oxidation with water vapor was lower than that of FeO_x in the third oxidation with water vapor. In contrast, the addition of both Mo and Rh species into FeO_x improved the durability for the redox as well as the reactivity of hydrogen formation at low temperatures. Oxidation of Rh–Mo–FeO_x with water vapor formed hydrogen at temperatures higher than 500 K. In addition, the peak of the formation rate of hydrogen for Rh–Mo–FeO_x was positioned at a lower temperature (ca. 620 K), compared to those for Mo–FeO_x (at 660 K) and for FeO_x (at 700 K). The reactivity of Rh–Mo–FeO_x for the hydrogen formation through the oxidation with water vapor was kept high from the first oxidation to the fifth oxidation. These results implied that the addition of Mo cations into FeO_x prevented the sintering of Fe_3O_4 and/or iron metal during the repeated redox. It is likely that Rh species added into the iron oxides worked as the active sites for water molecules during the oxidation with water vapor, because the addition of Rh species into FeO_x enhanced hydrogen formation at low temperatures.

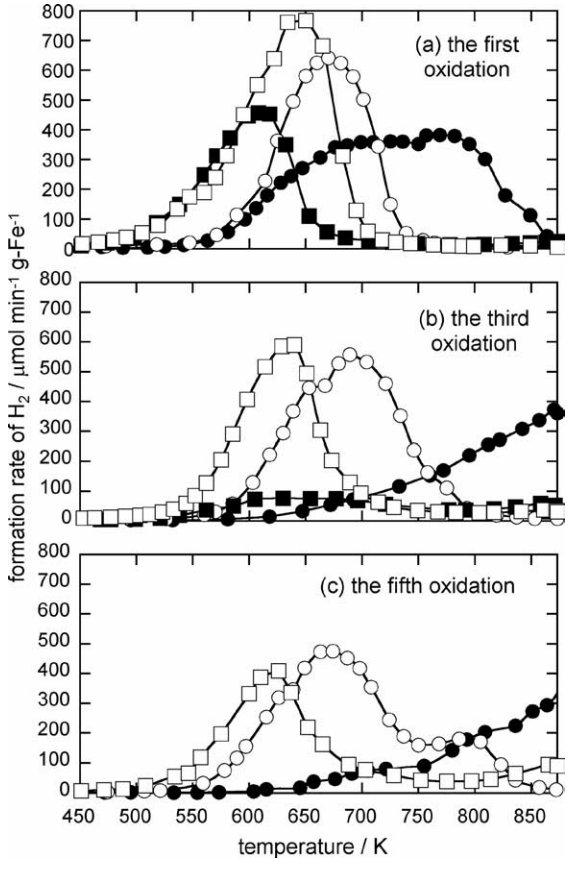

Fig. 1. Change of the formation rate of hydrogen as a function of temperatures during the oxidation of reduced iron oxides with water vapor. ●, FeO_x; ○, Mo–FeO_x; ■, Rh–FeO_x; □, Rh–Mo–FeO_x.

Apparent activation energies for the oxidation with water vapor of the iron oxide samples (FeO_x, Mo–FeO_x, and Rh–Mo–FeO_x) that had been reduced with hydrogen at 673 K were estimated. The redox reactions were performed with a gas-closed and gas-circulation system. The formation rates of hydrogen at the early period of the first oxidation with water vapor were measured at different temperatures in the range of 453 to 583 K. The apparent activation energies

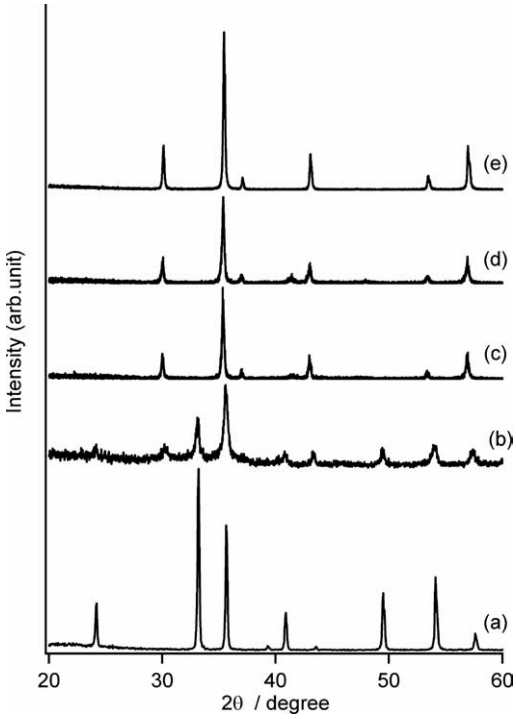

Fig. 2. XRD patterns of Rh–Mo–FeO_x before and after the oxidation with water vapor and the reference samples (Fe_2O_3 and Fe_3O_4). (a) Fe_2O_3 reference; (b) fresh Rh–Mo–FeO_x; (c) Rh–Mo–FeO_x after the first oxidation; (d) Rh–Mo–FeO_x after the third oxidation. (e) Fe_3O_4 reference.

for the first oxidation with water vapor of the FeO_x, Mo–FeO_x, and Rh–Mo–FeO_x were estimated to be 62, 59, and 37 kJ mol^{-1}, respectively. The addition of Rh species into the Mo–FeO_x decreased the apparent activation energy for the oxidation of iron metals with water vapor, while the activation energy did not change appreciably by the addition of Mo cations into FeO_x. These results implied that Rh species added into the iron oxides activated water molecules during the oxidation, while Mo cations in the samples could not activate them.

3.2. Characterization of Rh–Mo–FeO_x

Fig. 2 shows XRD patterns of Rh–Mo–FeO_x before and after the redox reactions and of the reference samples (Fe_2O_3 and Fe_3O_4). The XRD patterns of the used Rh–Mo–FeO_x were measured after the first oxidation and after the third oxidation with water vapor. The diffraction peaks due to Fe_2O_3 and Fe_3O_4 were observed in the XRD pattern of the fresh Rh–Mo–FeO_x sample (spectrum b), although the peaks due to Fe_3O_4 were significantly smaller than those due to Fe_2O_3. Any diffraction peaks assignable to compounds containing Mo or Rh species were not observed for the fresh Rh–Mo–FeO_x. These results implied that Rh and Mo species in the fresh Rh–Mo–FeO_x were highly dispersed. XRD patterns of Rh–Mo–FeO_x after the first oxidation (spectrum c) and after the third oxidation (spectrum d) were consistent with that of Fe_3O_4 (spectrum e). These Rh–Mo–FeO_x samples were reduced with hydrogen at 823 K and they subsequently were oxidized with water vapor at 873 K prior to the XRD measurements. Thus, iron metals which had been formed by the reduction of Rh–Mo–FeO_x with hydrogen were oxidized with water vapor completely into Fe_3O_4. A very weak peak due to crystallized Rh metal was observed at $2\theta = 41.5°$ for the XRD pattern of Rh–Mo–FeO_x after the third oxidation. In contrast, no diffraction signals due to the compounds containing Mo cations appeared in the XRD patterns of the Rh–Mo–FeO_x samples after the redox.

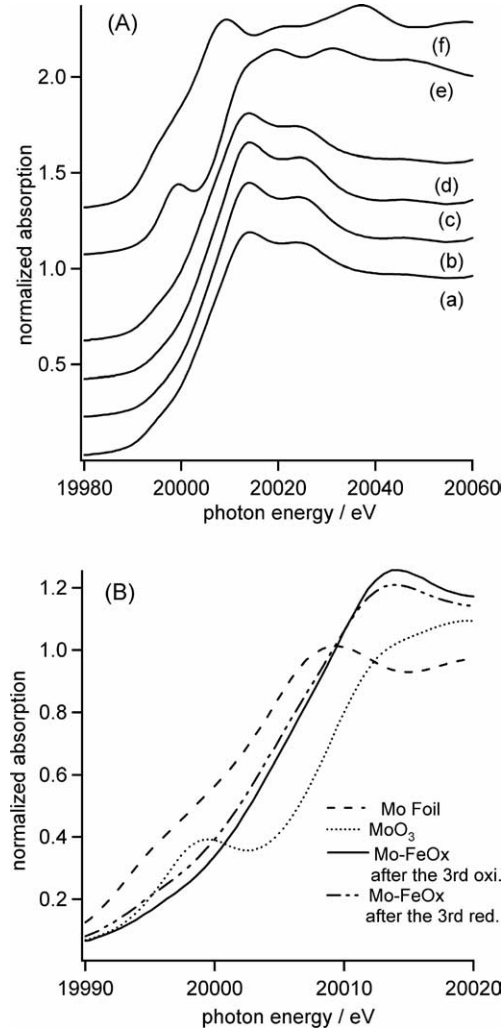

Fig. 3. Mo K-edge XANES spectra of Mo–FeO_x after the redox and of the reference samples (MoO_3 and Mo foil). (a)–(d) Mo–FeO_x samples: (a) after the first reduction; (b) after the first oxidation; (c) after the third reduction; (d) after the third oxidation. (e) MoO_3. (f) Mo foil.

As described earlier, the addition of Mo cations into FeO_x prevented the deactivation for the hydrogen formation through the oxidation of iron metals with water vapor. The structure of Mo cations in Mo–FeO_x could not be clarified by XRD studies. Thus, Mo K-edge XANES and EXAFS for Mo–FeO_x were measured in order to examine the local structures around Mo atoms added in FeO_x. Fig. 3 shows Mo K-edge XANES spectra of Mo–FeO_x after the redox and of

the reference samples (MoO_3 and Mo foil). The spectra of Mo–FeO_x were measured after the reduction with hydrogen at 823 K or after the subsequent oxidation with water vapor at 873 K. Fig. 3B shows the threshold of XANES spectra of these samples in an energy range of 19990 to 20020 eV. XANES spectra for all the Mo–FeO_x samples (spectra a–d) were similar to one another regardless of different treatments for the samples (after the reduction with hydrogen or after the oxidation with water vapor). These spectra of Mo–FeO_x were not consistent with that of MoO_3 (spectrum e) or that of Mo foil (spectrum f). It is well accepted that the position of threshold for XANES spectra of any metal species is sensitive to the oxidation states of the corresponding metal species; i.e., the threshold of XANES spectra of the metal species is shifted to higher energy with the higher oxidation state of the metal species [11–13]. The threshold of XANES spectra shown in Fig. 3B was positioned to higher energy in the following order of Mo foil < Mo–FeO_x < MoO_3, suggesting that the oxidation number of Mo cations in the Mo–FeO_x after the redox was lower than 6+ (VI) and higher than zero [14,15]. It was reported that Mo cations were stabilized on the B sites in the ferrites of the formula $Mo_xFe_{3-x}O_4$ when Mo cations were added into Fe_3O_4 [16,17]. The oxidation number of Mo cations in the ferrites was evaluated to be 3+ (III) or 4+ (IV). The present results of the XANES spectra of Mo–FeO_x were consistent with these previous reports. It should be noted that the threshold of XANES spectra for the Mo–FeO_x after the reduction with hydrogen was positioned at slightly lower energy compared to that for the Mo–FeO_x after the oxidation with water vapor. Thus, the fraction of Mo^{3+} in all the Mo cations (Mo^{3+} and Mo^{4+}) in the Mo–FeO_x after the reduction with hydrogen would be higher than that in the Mo–FeO_x after the oxidation with water vapor.

Fig. 4 shows Mo K-edge k^3-weighted EXAFS of Mo–FeO_x after the redox. The EXAFS spectrum for Mo–FeO_x after the first reduction (spectrum a) was similar to that of Mo–FeO_x after the third reduction (spectrum c). In addition, the EXAFS spectrum for Mo–FeO_x after the first oxidation (spectrum b) was consistent with that of Mo–FeO_x after the third oxidation (spectrum d). The spectra of Mo–FeO_x after the reduction were different from those of Mo–FeO_x after the oxidation. Thus, the local structure around Mo atoms in Mo–FeO_x after the reduction with hydrogen was changed by the oxidation with water vapor; however, it was recovered again by the subsequent reduction of the Mo–FeO_x with hydrogen, i.e., the reversible change of the local structure around Mo cations during the repeated redox of Mo–FeO_x. XANES spectra of Mo–FeO_x showed that the fraction of Mo^{3+} in all the Mo cations (Mo^{3+} and Mo^{4+}) depended on the state of the Mo–FeO_x (after the oxidation with water vapor or after the reduction with hydrogen). The change of the local structures around Mo cations in Mo–FeO_x during the repeated redox must result from the redox between Mo^{3+} and Mo^{4+} in the ferrites $Mo_xFe_{3-x}O_4$.

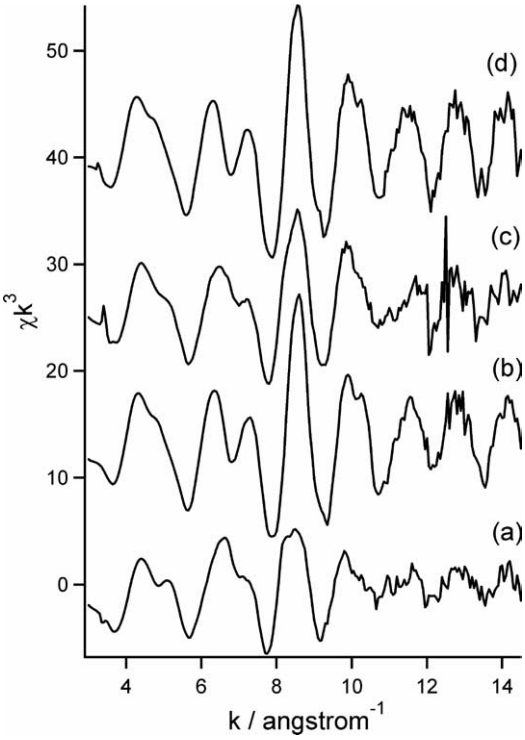

Fig. 4. Mo K-edge k^3-weighted EXAFS of Mo–FeO_x after the redox. (a) After the first reduction; (b) after the first oxidation; (c) after the third reduction; (d) after the third oxidation.

Fourier transforms for Mo K-edge k^3-weighted EXAFS of Mo–FeO_x after the redox were performed in order to obtain radial structural functions (RSFs) of the spectra. The RSFs for Mo–FeO_x are shown in Fig. 5. The RSFs for Mo–FeO_x after the reduction with hydrogen (spectra a and c) were different from those of Mo–FeO_x after the oxidation with water vapor (spectra b and d). Bouet et al. reported Fourier transforms of Mo K-edge EXAFS for the ferrites of the formula $Mo_xFe_{3-x}O_4$ [17]. The RSFs of the ferrites $Mo_xFe_{3-x}O_4$ were quite similar to ones shown in Fig. 5. Thus, Mo cations in Mo–FeO_x were always stabilized in the ferrites $Mo_xFe_{3-x}O_4$ during the repeated redox. It is likely that changes of the RSFs for Mo–FeO_x during the redox resulted from the change of the fraction of Mo^{3+} and Mo^{4+} in the ferrites $Mo_xFe_{3-x}O_4$.

Fig. 6 shows Rh K-edge XANES spectra of Rh–Mo–FeO_x after the redox, and the spectrum of Rh foil. The spectra of the Rh–Mo–FeO_x were measured after the reduction with hydrogen at 823 K or after the oxidation with water vapor at 873 K. The XANES spectrum of Rh–Mo–FeO_x after the first oxidation with water vapor (spectrum b) was consistent with that of Rh–Mo–FeO_x after the third oxidation (spectrum d). These spectra of Rh–Mo–FeO_x after the oxidation with water vapor were similar to that of Rh foil (spectrum e), suggesting that Rh species in the Rh–Mo–FeO_x after the oxidation with water vapor were present as Rh metal. On the other hand, XANES spectra of Rh–Mo–FeO_x after the reduction with hydrogen (spectra a and c) were different from that of Rh foil. Thus, Rh species in the

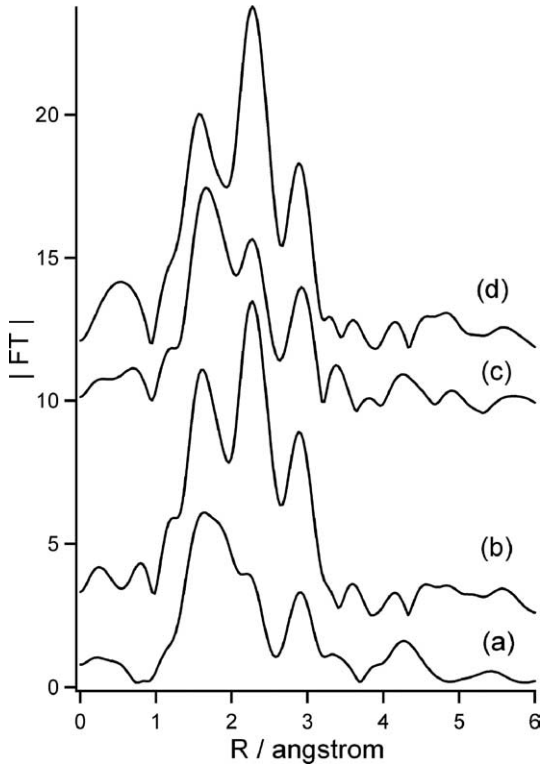

Fig. 5. Fourier transforms of Mo K-edge k^3-weighted EXAFS of Mo–FeO_x after the redox. (a) After the first reduction; (b) after the first oxidation; (c) after the third reduction; (d) after the third oxidation.

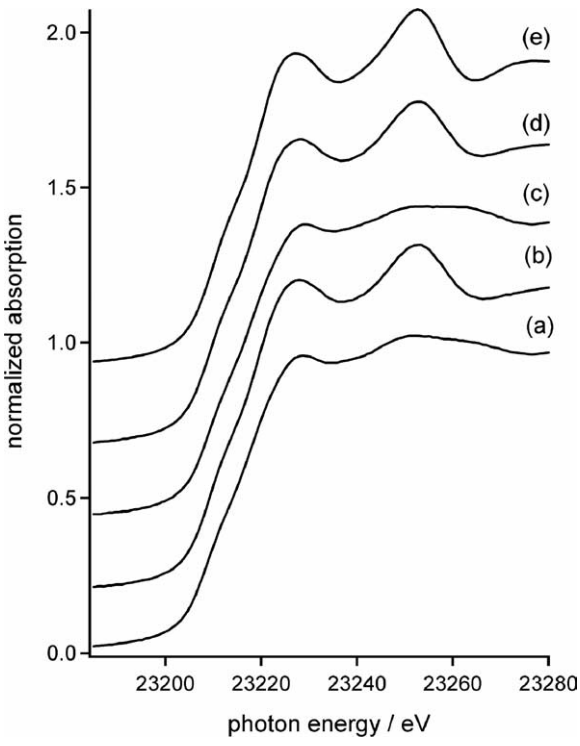

Fig. 6. Rh K-edge XANES spectra of Rh–Mo–FeO_x after the redox and of Rh foil. (a–d) Rh–Mo–FeO_x: (a) after the first reduction; (b) after the first oxidation; (c) after the third reduction; (d) after the third oxidation. (e) Rh foil.

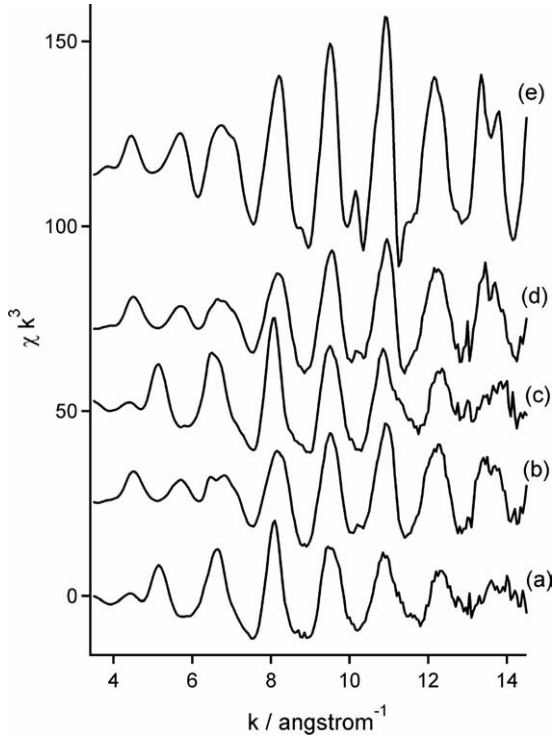

Fig. 7. Rh K-edge k^3-weighted EXAFS of Rh–Mo–FeO_x after the redox and of Rh foil. (a–d) Rh–Mo–FeO_x: (a) after the first reduction; (b) after the first oxidation; (c) after the third reduction; (d) after the third oxidation. (e) Rh foil.

Rh–Mo–FeO_x after the reduction with hydrogen were not crystallized Rh metal. It should be noted that the threshold for XANES spectra of the Rh–Mo–FeO_x after the reduction with hydrogen was consistent with that of Rh foil. This result implied that Rh species in the Rh–Mo–FeO_x after the reduction with hydrogen were of zero valent, although they were not Rh metal crystallite itself. As will be described below in detail, Rh species in the Rh–Mo–FeO_x after the reduction with hydrogen were present as Rh–Fe alloys. Therefore, Rh K-edge XANES spectra of the Rh–Mo–FeO_x after the reduction with hydrogen were assignable to that of Rh–Fe alloys.

Fig. 7 shows Rh K-edge k^3-weighted EXAFS of Rh–Mo–FeO_x after the reduction with hydrogen or after the successive oxidation with water vapor, and EXAFS of Rh foil. Fourier transforms of these EXAFS spectra (RSFs) were shown in Fig. 8. Fourier transforms were performed over a k range of 3.5 to 14.5 $Å^{-1}$. EXAFS oscillations for the Rh–Mo–FeO_x after the first oxidation (spectrum b in Fig. 7) and after the third oxidation (spectrum d) were compatible with that for Rh foil (spectrum e), although the intensity of EXAFS oscillation for the Rh–Mo–FeO_x was smaller than that for Rh foil. In addition, the RSFs of the Rh–Mo–FeO_x after the oxidation with water vapor (spectra b and d in Fig. 8) were similar to that for Rh foil (spectrum e). Thus, Rh species in the Rh–Mo–FeO_x after the oxidation with water vapor were present as Rh metal crystallites. On the other hand, EXAFS spectra of Rh–Mo–FeO_x after the reduction

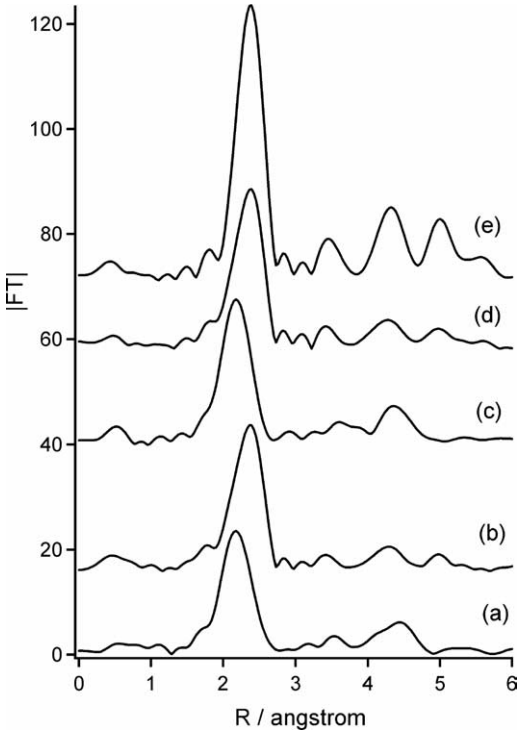

Fig. 8. Fourier transforms of Rh K-edge k^3-weighted EXAFS of Rh–Mo–FeO_x after the redox and of Rh foil. (a–d) Rh–Mo–FeO_x: (a) after the first reduction; (b) after the first oxidation; (c) after the third reduction; (d) after the third oxidation. (e) Rh foil.

with hydrogen (spectra a and c in Fig. 7) were different from that of Rh foil (spectrum e). The envelope function of the EXAFS for the Rh–Mo–FeO_x after the reduction had the maximum at a k value of 7–9 $Å^{-1}$, while the maximum of the envelope function for Rh foil was positioned at a k value of 9–12 $Å^{-1}$. This result implied that Rh atoms in the Rh–Mo–FeO_x after the reduction with hydrogen were surrounded by lighter atoms than Rh, i.e., Fe atoms. RSFs of the Rh–Mo–FeO_x in Fig. 8 also supported this idea. The intense peak was observed at 2.1 Å in the RSFs of the Rh–Mo–FeO_x after the reduction with hydrogen (spectra a and c in Fig. 8), while a strong peak due to a specific Rh–Rh bond appeared at 2.3 Å in the RSF of Rh foil. Thus, Rh atoms in the Rh–Mo–FeO_x after the reduction with hydrogen were surrounded by Fe atoms, i.e., the formation of Rh–Fe alloys.

The local structures around Rh atoms in the Rh–Mo–FeO_x during the redox were examined furthermore by curve fitting for Rh K-edge EXAFS. Inversely Fourier-transformed data for the Fourier peak at a R range of 1.7–2.9 Å on the RSFs of Rh–Mo–FeO_x in Fig. 8 were analyzed by a curve-fitting method. The structural parameters evaluated by the curve fitting are listed in Table 1. The strong peak in the RSFs for the Rh–Mo–FeO_x after the reduction with hydrogen could be assigned to a specific Rh–Fe bond. This result indicates the formation of Rh–Fe alloys in the Rh–Mo–FeO_x after the reduction with hydrogen. On the other hand, the peak in the RSF of the Rh–Mo–FeO_x after the oxidation with water vapor could be assigned to a specific

Table 1
Curve-fitting results for Rh K-edge EXAFS of Rh–Mo–FeO_x

Condition	Shell	C.N.[a]	R[b] (Å)	σ[c] (Å)
After the first reduction	Rh–Fe	6.6 ± 1.0	2.55	0.057
After the first oxidation	Rh–Rh	5.9 ± 0.4	2.66	0.058
After the third reduction	Rh–Fe	7.4 ± 0.6	2.55	0.056
After the third oxidation	Rh–Rh	6.2 ± 0.5	2.67	0.056

[a] Coordination number.
[b] Interatomic distance.
[c] Debye–Waller factor.

Table 2
Results of adsorption of H_2 and N_2 on the iron oxide samples

Samples	Surface area[a] ($m^2\,g^{-1}$)		H_2 ads.[b] ($\mu mol\,g^{-1}$)
	Fresh	Reduced	
FeO_x	36	11	54
Mo–FeO_x	77	54	46
Rh–Mo–FeO_x	63	40	40

[a] Specific surface area estimated by N_2 adsorption at 77 K with BET methods.
[b] Hydrogen was adsorbed on the samples reduced with hydrogen. Adsorbed amounts of H_2 were estimated from the isotherm assuming that hydrogen was adsorbed atomically on a metal atom with Langmuir-typed adsorption.

Rh–Rh bond in Rh metal crystals. The coordination number of Rh–Rh bond for the Rh–Mo–FeO_x after the first oxidation was estimated to be 5.9. The coordination number of Rh–Rh bond did not change significantly after the third oxidation with water vapor. Thus, Rh metal crystallites present on the Rh–Mo–FeO_x after the oxidation with water vapor were not aggregated seriously during the repeated redox cycles.

In order to estimate the fraction of the metallic surface of FeO_x, Mo–FeO_x, and Rh–Mo–FeO_x after the first reduction with hydrogen, the adsorption of nitrogen and hydrogen on these samples was performed. These samples were reduced with hydrogen at 673 K prior to the adsorption experiments. The specific surface areas of the samples were evaluated by BET methods of nitrogen adsorption at 77 K. Hydrogen adsorption on these samples was performed at 273 K. On the basis of these results, the fraction of the metallic surface area to the specific surface area of these samples after the reduction with hydrogen was evaluated. The results are shown in Table 2. Specific surface areas of the fresh FeO_x, Mo–FeO_x and Rh–Mo–FeO_x were estimated to be 36, 77, and 63 $m^2\,g^{-1}$, respectively. The specific surface areas for all the samples decreased after the first reduction with hydrogen. Nevertheless, the decrease in the surface areas of Mo–FeO_x and Rh–Mo–FeO_x after the first reduction with hydrogen was not so serious as that of FeO_x; that is, the specific surface areas of Mo–FeO_x (54 $m^2\,g^{-1}$) and Rh–Mo–FeO_x (40 $m^2\,g^{-1}$) were significantly larger than that of FeO_x (11 $m^2\,g^{-1}$). This result suggests that Mo cations added into FeO_x prevented the sintering of iron metal particles during the reduction with hydrogen.

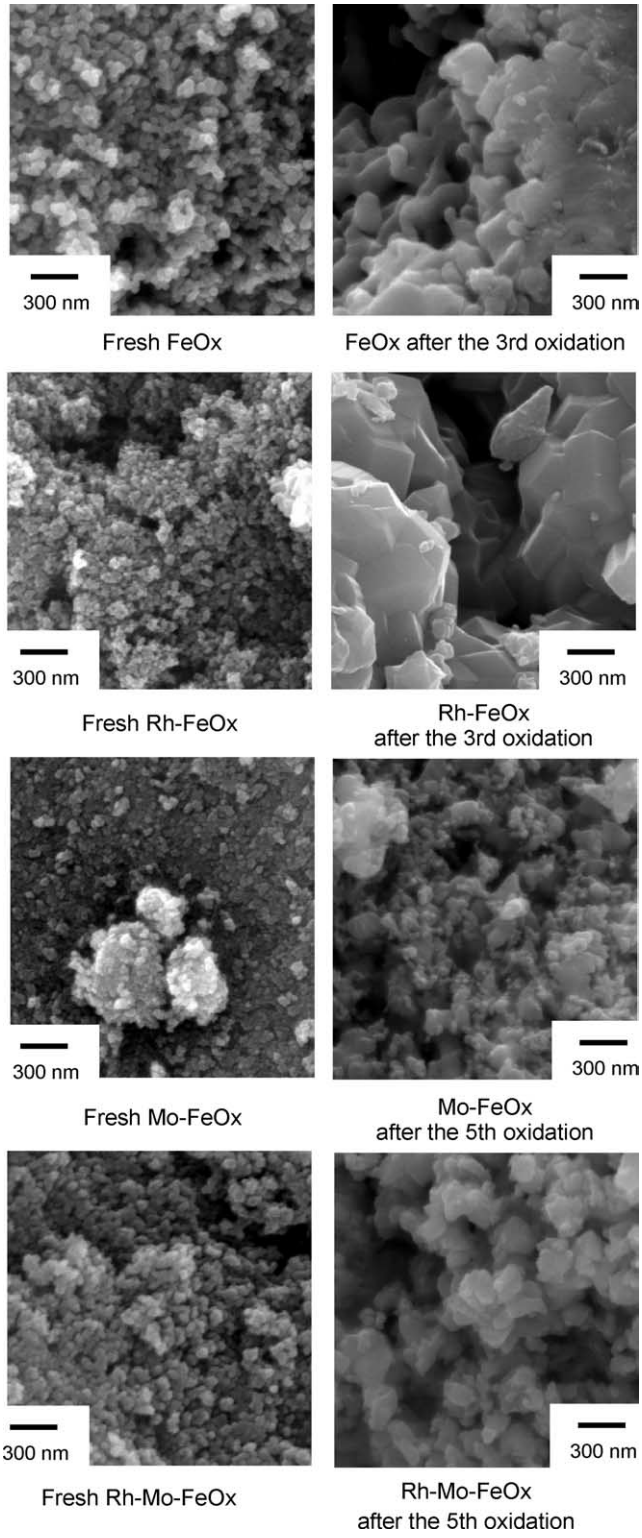

Fig. 9. SEM images of FeO_x, Rh–FeO_x, Mo–FeO_x, and Rh–Mo–FeO_x samples before and after the redox.

Fig. 9 shows SEM images of FeO_x, Rh–FeO_x, Mo–FeO_x, and Rh–Mo–FeO_x before and after the redox. All the fresh iron oxide samples shown in Fig. 9 were composed of Fe_2O_3 particles with diameters of 20 to 30 nm. After the third redox cycles of FeO_x, particles of Fe_3O_4 and/or iron metal in FeO_x were aggregated significantly to form particles larger than 200 nm. The aggregation of iron species (Fe_3O_4 and/or iron metal) after the third redox cycles was more serious in the case of Rh–FeO_x. The particle size of Rh–FeO_x after the third redox cycles was significantly larger than that of FeO_x after the third redox cycles. These results implied that the addition of Rh species into FeO_x promoted the sintering of Fe_3O_4 and/or iron metal during the redox. As described in Fig. 1, Rh–FeO_x was deactivated more quickly for the hydrogen formation through the oxidation with water vapor than FeO_x; i.e., the formation rate of hydrogen in the third oxidation of Rh–FeO_x with water vapor was lower than that for FeO_x in the third oxidation. This rapid deactivation of Rh–FeO_x would result from the serious aggregation of iron species. In contrast, average particle sizes of the Mo–FeO_x and Rh–Mo–FeO_x were relatively smaller even after the fifth redox cycles. Thus, we concluded that Mo cations added into FeO_x prevented the sintering of iron species during the repeated redox reactions.

The results of the hydrogen adsorption at 273 K on FeO_x, Mo–FeO_x, and Rh–Mo–FeO_x after the reduction with hydrogen (Table 2) would provide a relative fraction of metal surface of these samples, while whole surface areas of these samples were estimated by nitrogen adsorption at 77 K. The amounts of hydrogen adsorbed on the Mo–FeO_x (46 μmol g^{-1}) and Rh–Mo–FeO_x (40 μmol g^{-1}) after the reduction with hydrogen were smaller than that on the FeO_x (54 μmol g^{-1}) after the reduction with hydrogen, although the specific surface areas for the Mo–FeO_x (54 m^2 g^{-1}) and Rh–Mo–FeO_x (40 m^2 g^{-1}) were significantly larger than that for the FeO_x (11 m^2 g^{-1}). As described earlier, XANES and EXAFS spectra indicated that Mo species were present as the ferrites $Mo_xFe_{3-x}O_4$ and Rh species were stabilized as Rh–Fe alloys in the samples after the reduction with hydrogen. As for the hydrogen adsorption at 273 K on the iron oxide samples after the reduction with hydrogen, hydrogen atoms would be adsorbed on metallic sites of zero valent, i.e., Fe-metal sites on the FeO_x and Mo–FeO_x, and Fe-metal sites and Rh-metal sites on the Rh–Mo–FeO_x. The results in Table 2 implied that the fraction of metal surface area in the whole surface area of the Mo–FeO_x and Rh–Mo–FeO_x after the reduction with hydrogen was very low compared with the fraction of metal surface for the FeO_x after the reduction with hydrogen. Thus, considerable fractions of the surface of the iron metal particles in the Mo–FeO_x and Rh–Mo–FeO_x after the reduction with hydrogen would be covered with the ferrites $Mo_xFe_{3-x}O_4$. The ferrites $Mo_xFe_{3-x}O_4$ that are localized on the surface of iron metal particles in the Mo–FeO_x and Rh–Mo–FeO_x after the reduction with hydrogen should inhibit the contact between iron metal particles during the repeated redox. We believed that this is the main reason why the addition of Mo cations into the iron oxides prevented the sintering of iron species (Fe_3O_4 and/or iron metal) during the redox.

4. Conclusion

We concluded as follows based on the results described above:

1. The addition of Rh species to iron oxides enhanced the formation of hydrogen at low temperatures through the oxidation of iron metal with water vapor. The addition of Rh to the iron oxide samples decreased apparent activation energy for the hydrogen formation. However, Rh species in iron oxides promoted sintering of iron species during the redox. The addition of Mo cations to Rh–FeO_x prevented the sintering of iron species during the redox. The Rh–Mo–FeO_x could produce hydrogen repeatedly through the redox.
2. Rh species in Rh–Mo–FeO_x were present as Rh metal after the oxidation with water vapor, whereas they were present as Rh–Fe alloys after the reduction with hydrogen.
3. Mo cations in Rh–Mo–FeO_x and Mo–FeO_x were always stabilized in the ferrites $Mo_xFe_{3-x}O_4$ during the redox. The surface of iron metal particles in Rh–Mo–FeO_x and Mo–FeO_x after the reduction with hydrogen was covered with the ferrites $Mo_xFe_{3-x}O_4$. The ferrites $Mo_xFe_{3-x}O_4$ inhibited the contact between iron metal particles during the redox.

References

[1] S. Poulston, N.J. Price, C. Weeks, M.D. Allen, P. Parlett, M. Steinberg, M. Bowker, J. Catal. 178 (1998) 658.
[2] G. Costentin, J.C. Lavalley, F. Studer, J. Catal. 200 (2001) 360.
[3] S. Golunski, R. Rajaram, N. Hodge, G.J. Hutchings, C.J. Kiely, Catal. Today 72 (2002) 107.
[4] D.G. Barton, S.L. Soled, G.D. Meitzner, G.A. Fuentes, E. Iglesia, J. Catal. 181 (1999) 57.
[5] M.V. Twigg, M.S. Spencer, Top. Catal. 22 (2003) 191.
[6] J. Zao, Z. Feng, F.E. Huggins, N. Shar, G.P. Huffman, I. Wender, J. Catal. 148 (1994) 194.
[7] K. Otsuka, A. Mito, S. Takenaka, I. Yamanaka, Int. J. Hydrogen Energy 26 (2001) 191.
[8] K. Otsuka, C. Yamada, T. Kaburagi, S. Takenaka, Int. J. Hydrogen Energy 28 (2002) 335.
[9] K. Otsuka, T. Kaburagi, C. Yamada, S. Takenaka, J. Power Sources 122 (2003) 111.
[10] A. Ankudinov, B. Ravel, J.J. Rehr, S.D. Conradson, Phys. Rev. B 58 (1998) 7565.
[11] T. Tanaka, H. Yamashita, R. Tsuchitani, T. Funabiki, S. Yoshida, J. Chem. Soc., Faraday Trans. 1 84 (1988) 2987.
[12] T. Tanaka, T. Hanada, S. Yoshida, T. Baba, Y. Ono, Jpn. J. Appl. Phys. 32 (1993) 481.
[13] Y. Wang, Y. Ohnishi, T. Shishido, Q. Zhang, W. Yang, Q. Guo, H. Wan, K. Takehira, J. Catal. 220 (2003) 347.
[14] W. Ding, S. Li, G.D. Meitzner, E. Iglesia, J. Phys. Chem. B 105 (2001) 506.
[15] K. Asakura, Y. Noguchi, Y. Iwasawa, J. Phys. Chem. B 103 (1999) 1051.
[16] B. Domenichini, D. Aymes, P. Perriat, B. Gillot, Mater. Chem. Phys. 39 (1994) 80.
[17] L. Bouet, Ph. Tailhades, A. Rousset, K.R. Kannan, M. Verelst, G.U. Kulkarni, C.N.R. Rao, J. Solid State Chem. 102 (1993) 414.